# Performance Metrics for Nanofiltration-based Selective Separation for Resource Extraction and Recovery

**Ruoyu Wang**
Vanderbilt University
**Rongrong He**
Shanghai Advanced Research Institute
**Tao He**
Advanced Research Institute, Chinese Academy of Sciences
**Menachem Elimelech**
Yale University https://orcid.org/0000-0003-4186-1563
**Shihong Lin** ( shihong.lin@vanderbilt.edu )
Vanderbilt University

**Analysis**

**Keywords:**

**Posted Date:** October 5th, 2022

**DOI:** https://doi.org/10.21203/rs.3.rs-1972307/v1



**Additional Declarations:** There is **NO** Competing Interest.

**Version of Record:** A version of this preprint was published at Nature Water on March 9th, 2023. See the published version at https://doi.org/10.1038/s44221-023-00037-0.

# Abstract

Membrane filtration has been widely adopted in various water treatment applications, but its use in selective solute separation for resource extraction and recovery is an emerging research area. When a membrane process is applied for solute-solute separation to extract solutes as the product, the performance metrics and process optimization strategies should differ from a membrane process for water production because of separation goals are fundamentally different. In this analysis, we used lithium (Li) magnesium (Mg) separation as a representative solute-solute separation to illustrate the deficiency of existing performance evaluation framework developed for water-solute separation using nanofiltration (NF). We performed coupon and module scale analyses of mass transfer to elucidate how membrane properties and operating conditions affect the performance of Li/Mg separation in NF. Notably, we identified an important operational tradeoff between Li/Mg selectivity and Li recovery, which is critical for process optimization. We also established a new framework for evaluating membrane performance based on the success criteria of Li purity and recovery. This analysis lays the theoretical foundation for performance evaluation and process optimization for NF-based selective solute separation.


# Introduction

Selective solute-solute separation has become a research frontier due to its potential applications in resource extraction and recovery.[1,2] The technological progress made in membrane-based solute-water separation over the past half century, particularly in reverse osmosis (RO) and nanofiltration (NF), has enabled energy-efficient desalination and water purification.[3,4] In those applications, water is the primary product whereas the solutes are the unwanted constituents to be rejected by membranes (Fig. 1A). In seawater or brackish water desalination, the rejected solutes are mainly salts, while in wastewater reuse, the rejected solutes include both salts and organic substances. The ideal membranes for these applications should have a high water-solute selectivity, i.e., they should have high water permeability while maintaining low solute permeability, leading to fast water production and high solute rejection.[3,5] Extensive efforts have been devoted to developing membranes with high water-solute selectivity.[5,6] To date, commercial RO/NF membranes have adequate water-solute selectivities for delivering reasonably good performance in desalination and water purification.[7,8]

Because RO membranes reject most solutes to a great extent and indiscriminately, pressure driven membrane-based selective solute-solute separation relies on NF which differentiates the rejections of solutes based on their physicochemical properties (Fig. 1B). In general, NF-based solute-solute separation can be classified into two major categories (Fig. 1C). In the first category, the primary product is water, and the role of solute-solute separation is to *improve* the NF-based water treatment processes. For instance, in NF-based water softening, hardness ions ($Ca^{2+}$ and $Mg^{2+}$) are rejected whereas monovalent ions (e.g., $Na^{+}$ and $K^{+}$) can readily pass through.[9,10] NF has also been used to selectively remove micropollutants without removing benign mineral ions.[11,12] The ability to achieve selective solute-solute

separation in these contexts can lead to a desired product water quality (e.g., reserving nutrient ions for fertigation), prevention of mineral scaling in subsequent desalination processes, and/or energy saving via reducing transmembrane osmotic pressure difference.

The second category of NF-based selective solute-solute separation aims at enabling the extraction of target solutes as the primary product. For example, when strong acid or base is used to recover cationic or anionic adsorbates from polymeric or mineral adsorbents, NF can be applied to concentrate the adsorbates (in the retentate) and recover acid or base (in the permeate) for reuse. A similar application of this type for NF is dye recovery from textile wastewater, where dye molecules are retained and concentrated as the target solutes.[13] One potentially prominent NF application of the second category is lithium (Li) extraction from brines rich in magnesium (Mg).[14]

The conventional method for Li production from brine is based on evaporation and chemical precipitation, which typically requires that the brine has a low Mg to Li ratio (MLR).[15,16] In recent years, integration of membrane processes into the treatment trains has received increasing interest for process intensification, and for enabling Li extraction from brines with high MLR.[14] A representative treatment train includes an evaporative process for precipitating out Na and K salts, an NF process for separating Li and Mg, an RO process to concentrate the Li-rich NF permeate, and a final precipitation process for generating $Li_2CO_3$ as the product (Fig. 1D).[17] NF-based Li/Mg separation is the most critical and technically challenging compared to the other unit processes that are relatively mature. Thus, many efforts have been devoted in recent years to develop high-performance NF membranes for Li/Mg separation.[18–24]

But what exactly is a good NF membrane for Li/Mg separation, or more generally, for any solute-solute separation? As the treatment goal is no longer simple separation of solute from water, the conventional framework of membrane evaluation based on water-solute selectivity is insufficient. In most papers on developing solute-solute separation membranes, performance was evaluated based on solute-solute selectivity and water permeability.[18–24] The selectivity of solute A over solute B, $S_{A/B}$, is defined as[25]

$$S_{A/B} = \frac{1 - R_A}{1 - R_B} = \frac{J_A / c_{f,A}}{J_B / c_{f,B}} \quad (1)$$

where $R_A$ ($R_B$), $J_A$ ($J_B$) and $c_{f,A}$ ($c_{f,B}$) are the apparent rejection, solute flux, and feed concentration of solute A (or B), respectively. $S_{A/B}$ is also called separation factor. The solute flux and feed concentration can be based on either mass or mole as long as the concentrations are consistent within the equation. In the following discussion, we will use mass-based definitions as adopted by most literature, although mole-based definitions are mechanistically more meaningful.

In this Analysis, we will show that $S_{A/B}$ alone is not a sufficient performance metric for evaluating an NF membrane or process for selective solute-solute separations for resource recovery. While the principle

should be generally applicable, we focus the current analysis on the specific application of Li/Mg separation to provide a concrete illustration. We start our analysis by evaluating the success criteria for Li/Mg separation and provide a critical analysis of literature data. We then perform coupon and module scale analysis to elucidate important operating and material considerations in NF-based Li/Mg separation. Finally, we introduce and discuss two important tradeoffs that will guide future process optimization and membrane development to achieve high-performance Li/Mg separation.

## Why Is Selectivity Not A Sufficient Metric?

Assessing the adequacy of the metric $S_{A/B}$ requires first defining a successful Li/Mg separation. Because the purpose of the separation is to extract Li from a Li/Mg mixture, the success criteria should have two aspects: purity and recovery (Fig. 1E). Considering a simplified scenario with only $Li^+$ and $Mg^{2+}$ cations, the permeate Li purity, $\eta_{Li}$, is defined as the mass fraction of cations in the permeate that are $Li^+$:

$$\eta_{Li} = \frac{c_{p,Li}}{c_{p,Li} + c_{p,Mg}}$$

2

where $c_{p,Li}$ and $c_{p,Mg}$ are the $Li^+$ and $Mg^{2+}$ concentrations in the permeate, respectively. The importance of Li purity is obvious as improving Li purity is the motivation for performing Li/Mg separation. A permeate with low Li purity will result in $Li_2CO_3$ precipitate containing unacceptable level of $MgCO_3$ impurity. For a feed solution of a given MLR, $\eta_{Li}$ relates to the Li/Mg selectivity, $S_{Li/Mg}$, via the following equation:

$$\eta_{Li} = \frac{1}{1 + MLR/S_{Li/Mg}}$$

3

The second important success criterion is Li recovery, defined as the mass fraction of $Li^+$ in the feed that is eventually recovered in the permeate. Specifically, Li recovery, $LiR$, can be quantified as

$$LiR \equiv \frac{Q_p c_{p,Li}}{Q_f c_{f,Li}} = WR(1 - R_{Li})$$

4

where $Q_p$ and $Q_f$ are the volumetric permeate flowrate and influent flowrate of the feed stream, respectively; $c_{p,Li}$ and $c_{f,Li}$ are the Li concentrations in the permeate and feed influent, respectively; $WR$ is water recovery; and $R_{Li}$ is Li rejection. Both $WR$ and $R_{Li}$ are module-scale performance metrics. As we will show shortly, using $R_{Li}$ evaluated with membrane coupons for module-scale analysis can lead to inaccurate or even unphysical results. With the definitions of Li purity and recovery, it becomes apparent that a successful Li/Mg separation should recover the majority of Li from the feed solution and at the

same time produce a permeate with a high Li purity (Fig. 1E). In other words, attaining only high Li recovery or high Li purity alone is undesirable for the purpose of Li extraction (Fig. 1F).

We summarize and analyze literature data on the performance of NF membranes used or developed for Li/Mg separation. We also tested the performance of several commercial membranes (NFX, NF90, and NF270). Both the literature data and results from our experiments are compiled in Fig. 2A, B, C, D (see also Table S1). The feed MLR spans a wide range from 5:1 to 120:1 and the $Mg^{2+}$ concentrations vary by nearly two orders of magnitude (Fig. 2A). The feed composition is critical as it affects Li/Mg selectivity and directly impacts Li purity via Eq. 3.

The rejections of $Li^+$ and $Mg^{2+}$ span a wide range of values (Fig. 2B). The rejections of $Mg^{2+}$ are typically higher than 70% and can even reach 99.9%. The $Li^+$ rejection ($R_{Li}$) varies from − 140–87%. Negative rejection of highly permeable ions ($Li^+$ in this case) is a result of maintaining Donnan equilibrium and is common in NF when the feed solution mixture has an abundance of less permeable co-ions ($Mg^{2+}$ in this case) that are strongly rejected and counter-ions ($Cl^-$ in this case) that can easily permeate through the membrane.[10,26,27] The permeation of $Cl^-$ promotes the transport of the highly permeable cation, $Li^+$, to maintain charge neutrality in the permeate solution, thereby resulting in a permeate with even higher $Li^+$ concentration than that of the feed.

The Li/Mg selectivity, $S_{Li/Mg}$, is strongly sensitive to $Mg^{2+}$ rejection, especially when $Mg^{2+}$ rejection is high (Fig. 2C). This dependence is also obvious from the definition of $S_{Li/Mg}$ (Eq. 1) in which the denominator is $1 - R_{Mg}$. The Li/Mg selectivity and the feed MLR together determine the permeate Li purity, which ranges from below 10% to over 90% (Fig. 2D). The high sensitivity of $S_{Li/Mg}$ to $R_{Mg}$ suggests that a very high $S_{Li/Mg}$ can be achieved even if $Li^+$ are well rejected, provided that $Mg^{2+}$ rejection is near perfect. This property of $S_{Li/Mg}$ renders it an insufficient performance metric as it is strongly biased toward the purity aspect of the success criteria while overlooking the factor of Li recovery.

To illustrate the inadequacy of selectivity as a performance metric, a heuristic comparison between two scenarios with the exact same Li/Mg selectivity (50) is provided in Table 1. Two different separations with the same selectivity fall on the same Li/Mg selectivity line in Fig. 2B and have the same permeate purity for a given feed MLR. The $R_{Li}$ and $R_{Mg}$ are −80% and 96.4%, respectively, in the first scenario, and 95% and 99.9% in the second scenario. Li recovery, $LiR$, is estimated by Eq. 4 to be 90% for the first scenario but only 2.5% for second scenario when $WR$ is 50%. The extreme difference of $LiR$ for the two separations with precisely the same Li/Mg selectivity clearly demonstrates why selectivity is an inadequate metric. Because of the high sensitivity of Li/Mg selectivity to $R_{Mg}$, especially when $R_{Mg}$ approaches 100%, a very high Li/Mg selectivity can be achieved even when $R_{Li}$ is unacceptably high for any Li recovery.

**Table 1:** Performance comparison of two scenarios with the same Li/Mg selectivity

| | | Scenario 1 | Scenario 2 |
|---|---|---|---|
| Li/Mg Selectivity | | 50 | |
| Purity | MLR=10 | 83.3% | |
| | MLR=50 | 50.0% | |
| $Li^+$ Rejection | | -80% | 95% |
| $Mg^{2+}$ Rejection | | 96.4% | 99.9% |
| LiR [(1)] | WR=50% | 90% | 2.5% |
| | WR=80% | 144% | 4.0% |

[(1)] The lithium recovery (LiR) calculated here is based on the to-be-disproved assumption of WR-independent $Li^+$ and $Mg^{2+}$ rejections.

Notably, applying Eq. 4 with a $WR$ of 80% in the first scenario predicts an unphysical $LiR$ of 144%. The emergence of this unrealistic prediction is attributable to the implicit assumption of a constant $R_{Li}$ when using Eq. 4. While an $R_{Li}$ of −80% is not uncommon in literature (Fig. 2B), those reported $R_{Li}$ values were measured using membrane coupons (i.e., $WR$ is nearly zero) with a certain feed solution composition. To achieve a $WR$ of 80% with membrane modules, however, the feed composition varies along the module due to the selective transport of water and ions. As we will show later, $R_{Li}$ depends on feed solution composition and water flux and thus cannot be -80% throughout the module. In other words, an $LiR$ >100% should not emerge in a module-scale analysis that correctly captures the mass transfer behavior, which is the focus of the next section.

## Module-scale Analysis Of Nf-based Li/mg Separation

Performing module-scale analysis requires a model to describe the local mass transfer in a differential element of the module. Such a model predicts the local fluxes of water and ions using applied pressure and local feed composition as the inputs. The module behavior can then be modeled via finite difference method to relate mass transfer in differential elements (see Section S1 for details). In this analysis, we employ the solution-diffusion-electromigration (SDEM) model due to its simplicity and ability to model fluxes of multiple components. The SDEM model assumes that any point inside the membrane is in thermodynamic equilibrium with a virtual bulk electrolyte solution that is charge neutral.[27–29] The virtual solution treatment is equivalent to applying a modified Nernst-Planck equation with the ion diffusion coefficient replaced by the ion permeability, which is the product of the partition and diffusion coefficients (Section S1).[29] The ion flux for species $i$, $J_i$, in the SDEM model is described using the modified Nernst-Planck equation:

$$J_i = -P_i \left( \frac{dc_i}{dx} + z_i c_i \frac{d\phi}{dx} \right)$$

5

where $P_i$ is the ion permeability, $c_i$ is the ion concentration in the virtual solution, $x$ is the transmembrane coordinate normalized by the membrane thickness, $z_i$ is the valence of species $i$, and $\phi$ is the local electrical potential in the virtual solution. Solving Eq. 5 yields the trans-membrane distributions of ion concentrations, electrical potential, and electrical field (Fig. 3A as an illustration), which enables calculating rejections in a local differential element.

The SDEM model is semi-empirical because $P_i$ is not constant but has a rather complex dependence on the feed composition. Comprehensive mechanistic models capable of describing multi-component transport are still under active development and they usually contain questionable assumptions and many fitting parameters. For simplicity, we employ a linear correlation to relate $P_i$ to feed composition:

$$P_i = \alpha_1 c'_{f,Li} + \alpha_2 c'_{f,Mg} + \alpha_3$$

6

where $c'_{f,Li}$ and $c'_{f,Mg}$ are the local interfacial feed concentrations of $Li^+$ and $Mg^{2+}$, and $\alpha_j$ are fitting coefficients. The local interfacial concentrations relate to the local bulk concentrations via concentration polarization (CP):

$$\frac{c'_{f,i} - c_{p,i}}{c_{f,i} - c_{p,i}} = \exp\left(\frac{J_w}{k_i}\right)$$

7

where $J_w$ is local water flux and $k_i$ is the mass transfer coefficient of species $i$. $J_w$ can be estimated using

$$J_w = P_w \left(\Delta P - \Delta \pi_m\right)$$

8

where $P_w$ is the water permeability, and $\Delta P$ and $\Delta \pi_m$ are the transmembrane difference of hydrostatic pressure and osmotic pressure, respectively. For relatively dilute solutions, the van't Hoff equation can be applied to relate $\Delta \pi_m$ to transmembrane concentration differences (Section S2).

We use the data of water flux and ion rejections of a polyelectrolyte membrane coupon measured with different feed compositions (Fig. 3B) as reported by He et al.[24] to extract the permeability of $Li^+$ ($P_{Li}$) and $Mg^{2+}$ ($P_{Mg}$) and determine the correlation coefficients in Eq. 6. The polyelectrolyte membrane (named LbL in Figs. 3B and 3C) was fabricated using layer-by-layer (LbL) deposition of poly sodium (4-styrenesulfonate) (PSS) and poly(allylamine) hydrochloride (PAH).[24] Additionally, we also measured the performance of commercial NF membranes using the same set of conditions (Section S3). The

correlations of ion permeability for these membranes are summarized in Table S2. In general, $P_{Li}$ is one to two orders of magnitude higher than $P_{Mg}$, and the linear correlations can provide reasonable predictions of the permeabilities extracted from the SDEM model using experimental data (Fig. 3C).

With a model to evaluate the local mass transfer in a differential element, we can now extend the analysis to module-scale by coupling different elements via species conservation (Section S1). Here, we base our illustrative analysis on the polyelectrolyte membrane and generate representative results to describe the module-scale behaviors in NF-based Li/Mg separation. Intuitively, the module behavior can be described as a spatial distribution of solution properties and separation performance along the direction of the feed flow. However, a more universal representation is to replace the position in the module with $WR$ (up to that position) because $WR$ increases as feed water flows past more membrane area.

As more water is recovered, the $Mg^{2+}$ concentration in the retentate (i.e., the solution remaining in the feed channel after partial water recovery) increases dramatically, whereas the retentate $Li^{+}$ concentration first increases and then decreases but overall remains low (Fig. 4A). The permeate concentrations of $Li^{+}$ and $Mg^{2+}$ consistently increase with increasing $WR$ (Fig. 4B). Here, we distinguish between the local and cumulative average permeate concentrations: the local concentrations are what could have been measured using a membrane coupon with the local feed composition, whereas the cumulative average concentrations consider the cumulative ion and water permeation preceding the position corresponding to the current $WR$ (i.e., $\int J_i dS / \int J_w dS$, where $dS$ is the differential membrane area). Correspondingly, the $Li^{+}$ and $Mg^{2+}$ rejections can also be defined locally and cumulatively (Fig. 4C). While the local $Li^{+}$ rejection can become strongly negative (like observations in membrane coupons), the cumulative average $Li^{+}$ rejection cannot, thereby preventing the erroneous inference of over 100% $LiR$ shown in Table 1.

The non-monotonic dependence of retentate $Li^{+}$ concentration on $WR$ (Fig. 4A inset) is a direct result of local $Li^{+}$ rejection transitioning from positive to negative as $WR$ increases (Fig. 4C). Despite the low (but positive) $R_{Li}$ at low $WR$, the $Li^{+}$ in the retentate is still concentrated with more water recovered, until $R_{Li}$ becomes negative at high $WR$. The strongly negative rejection of $Li^{+}$ in the range of high $WR$ is a result of both high local MLR ratio (Fig. 4D) and low local water flux due to diminishing driving force with increasing retentate osmotic pressure (Figure S1). Notably, both the cumulative average selectivity and local selectivity drop with increasing $WR$ (Fig. 4E) despite the progressively more favorable $Li^{+}$ permeation at higher $WR$ (Fig. 4C), which can be explained by the noticeable reduction of $R_{Mg}$ with increasing $WR$ (Fig. 4C inset) and the high sensitivity of $S_{Li/Mg}$ to $R_{Mg}$ (Eq. 1). The drop in local Li/Mg selectivity is a result not only of the varying retentate composition (Fig. 4A) but also the varying water flux, as selectivity could be substantially compromised when the water flux is too low (Section S4). Lastly, Li recovery, $LiR$, increases monotonically as more water is recovered (Fig. 4F).

# Performance Tradeoff In Nf Operation

From an operational perspective, the module-scale analysis reveals an intrinsic tradeoff between the (cumulative average) selectivity, $S_{Li/Mg}$, and Li recovery, $LiR$. For a single-stage NF process with a given applied pressure and influent feed flowrate, a higher $WR$ can be achieved by providing more membrane area. Increasing $WR$ increases $LiR$(Fig. 4F) but at the cost of reduced $S_{Li/Mg}$(Fig. 4E), resulting in the tradeoff between $S_{Li/Mg}$ and $LiR$ (Fig. 5A).

The characteristic curve quantifying the tradeoff between $S_{Li/Mg}$ and $LiR$, namely the operational tradeoff curve, depends on the applied pressure, $\Delta P$, which affects the water flux. At a low $\Delta P$, water permeates through the membrane at a slower rate. However, the ion fluxes are not affected proportionally due to the negligible advective ion transport in NF. Therefore, operating NF at lower $\Delta P$ enhances $Li^+$ permeation as compared to water permeation, which results in a higher $LiR$ at the same $WR$ and thereby shifts the tradeoff curve toward the right (see dash curves in Fig. 5A). This effect of enhanced $LiR$ at the same $WR$ is more prominent at a higher $WR$. Notably, the maximum $WR$ achievable with unlimited membrane area is also dependent on $\Delta P$, as water permeation stops when $\Delta \pi_m$reaches $\Delta P$. In the extreme case of applying only 1 bar, the maximum attainable $WR$ and $LiR$ are ~ 10% and ~ 22%, respectively.

In the range of low $WR$, $S_{Li/Mg}$ increases considerably as $\Delta P$ decreases from 8 bar to 4 bar, i.e., reducing $\Delta P$ and water flux in this range also shifts the tradeoff curves up (Fig. 5A). However, further reducing $\Delta P$ below 4 bar compromises $S_{Li/Mg}$ (see reflection of dash curves in Fig. 5A). With a $\Delta P$ of 1 bar, $S_{Li/Mg}$ becomes very low. While the cumulative average selectivity, $S_{Li/Mg}$, has a complex dependence on multiple factors (e.g., water flux, feed composition) that varies along the module, the non-monotonic dependence of $S_{Li/Mg}$ can be explained by the flux dependence of local selectivity (i.e., at the coupon scale with a fixed feed composition) as shown in Fig. 5B.

In the water flux regime typical of NF (gray region in Fig. 5B), local Li/Mg selectivity decreases monotonically with increasing water flux due to concentration polarization (CP). Specifically, because $Mg^{2+}$ ions are far better rejected than $Li^+$ ions, the accumulation of $Mg^{2+}$ near the membrane surface is more severe than $Li^+$, which results in a higher interfacial MLR at a higher water flux (Figure S3). A higher interfacial MLR is detrimental to local Li/Mg selectivity which is strongly sensitive to $Mg^{2+}$ rejection, because a heightened interfacial $Mg^{2+}$ concentration compromises $Mg^{2+}$ rejection (Figure S4). In the very low water flux regime (yellow region in Fig. 5B, untypical of NF), local Li/Mg selectivity drops dramatically with decreasing water flux due to the significantly reduced rejections of all ions because of the weakened “dilution effect”. Because $S_{Li/Mg}$ is much more sensitive to $Mg^{2+}$ rejection than to $Li^+$ rejection, reducing the rejections of all ions leads to a dramatic drop in $S_{Li/Mg}$.

Because selectivity is related to the permeate Li purity, $\eta_{Li}$, via Eq. 3, the tradeoff between $S_{Li/Mg}$ and $LiR$ presented in Fig. 5A can be directly converted to a tradeoff between $\eta_{Li}$ and $LiR$ for a given feed MLR (Figure S5). At a given applied pressure, the tradeoff between the two important performance metrics in Li/Mg separation suggests that recovering more $Li^+$ by using a larger membrane area will

inevitably yield a product permeate stream with a lower $\eta_{Li}$. Within the typical range of NF flux, $S_{Li/Mg}$ and $LiR$ can be simultaneously improved by operating NF at a lower pressure to reduce water flux. Additionally, the tradeoff curve can also be shifted toward a more favorable direction when a better membrane is used, with the definition of “better” to be discussed below.

## Performance Metrics Of Nf Membrane For Li/mg Separation

What exactly is a “better membrane” in the context of Li/Mg separation is an important question to the vibrant and growing community for developing high performance NF membranes for Li/Mg separation. While many previous papers in this field compare membrane performance in a plot of Li/Mg selectivity vs. water permeability ($S_{Li/Mg}$vs. $P_w$), we have demonstrated why $S_{Li/Mg}$ is an insufficient metric (Table 1). We have also shown that a higher water flux is detrimental to both Li selectivity (or purity) and recovery (Fig. 5). Therefore, a high $P_w$ seems at odds with the success criteria for Li/Mg separation.

Because selectivity is defined based on rejections which are less intrinsic than permeabilities, membrane performance is more commonly quantified based on permeabilities. Although one may rightfully argue that permeabilities are also not entirely intrinsic properties of membranes due to their dependence on feed composition, they are more intrinsic than rejections and are adopted in the most widely used framework for evaluating membrane performance for water-solute separation. Selectivity in water-solute separation is defined based on the ratio between water permeability ($P_w$) and solute permeability ($P_s$). The water/solute selectivity ($P_w/P_s$) is usually plotted against the water permeability ($P_w$) to illustrate the perm-selectivity of membranes.[7,30,31] However, such a performance evaluation framework based on $P_w/P_s$ vs. $P_w$ is clearly inappropriate for Li/Mg separation with very different success criteria compared to water-solute separation.

On the one hand, an ideal NF membrane for Li/Mg separation should allow fast $Li^+$ transport and slow $Mg^{2+}$ transport so that selective permeation of $Li^+$ over $Mg^{2+}$ can be achieved to maximize Li purity. On the other hand, an ideal NF membrane should also favor $Li^+$ permeation over water permeation to promote Li recovery. If water permeation is very fast yet $Li^+$ permeation is very slow, only a small fraction of $Li^+$ in the feed solution will end up in the permeate. Given these considerations, we propose that the performance of an NF membrane for Li/Mg separation should be evaluated based on two permeability ratios, $P_{Li}/P_{Mg}$ and $P_{Li}/P_w$ (Fig. 6). A high $P_{Li}/P_{Mg}$ favors Li/Mg selectivity and Li purity, whereas a high $P_{Li}/P_w$ favors Li recovery. These two permeability ratios directly correspond to the two success criteria in NF-based Li/Mg separation.

Like water-solute separation, a membrane with a higher $P_w$ can reduce the energy consumption and/or membrane area for a given feed flowrate, thereby reducing overall cost of the separation.[3,8] In Li/Mg separation, however, a higher $P_w$ is beneficial only if it does not compromise $P_{Li}/P_w$, because $LiR$ is likely more important as a performance metric than water flux or volume-specific energy consumption. In a bubble plot of $P_{Li}/P_{Mg}$ vs. $P_{Li}/P_w$, where $P_w$ may be quantified by the size of the “bubbles” (Fig. 6), an ideal membrane is a “big bubble” on the upper right of the plot. The concept of a performance upper

bound commonly employed for perm-selectivity in water-solute separation can also apply here to describe the tradeoff between Li purity and recovery. Future studies on developing high-performance NF membranes should aim to populate the bubble plot beyond the current upper bound line.

The $P_{Li}/P_{Mg}$ vs. $P_{Li}/P_w$ bubble plot should be used with caution when comparing membrane performance. Ideally, all data points in this plot should be obtained using the same feed composition and operating conditions, which is not necessarily the case across different studies. These testing conditions impact membrane performance, which is evident from the mild scattering of performance for a given membrane tested in different conditions (Fig. 6 and Table S3). Future studies on membrane development should converge to a unified testing protocol for performance comparison on the $P_{Li}/P_{Mg}$ vs. $P_{Li}/P_w$ bubble plot.

# Perspectives And Outlook

Our analysis demonstrates that the existing framework for evaluating NF performance in water treatment is inadequate for quantifying NF performance for selective solute-solute separation. The performance metrics in the existing framework mismatch the success criteria for selective solute-solute separation when the goal is to extract a target solute as the desired product. As an important application of NF-based selective solute-solute separation, Li/Mg separation is chosen as an example for illustrating such a mismatch and for developing a suitable framework for evaluating process and membrane performance. In the specific example of Li/Mg separation, the key performance metrics at the process level should be Li/Mg selectivity (or Li purity) and Li recovery—not water permeability as currently used. The consideration of these two metrics results in important tradeoff relations for operation optimization and membrane development.

From an operation perspective, process optimization of NF for Li/Mg separation should focus on Li purity and recovery which are constraint by a tradeoff relation (Fig. 5) that can serve as the technical foundation for process optimization. Factors that are critical in water treatment, such as energy consumption and membrane cost, are likely less important in Li/Mg separation due to Li being a commodity with a much higher economic value than water. From membrane development perspective, NF membranes for Li/Mg separation should be evaluated using the $P_{Li}/P_{Mg}$ vs. $P_{Li}/P_w$ bubble plot (Fig. 6), which captures membrane properties most relevant to the success criteria of Li/Mg separation.

While this analysis focuses on Li/Mg separation, other solute-solute separations with the objectives of solute recovery or extraction also require adapting the performance evaluation framework based on the application-dependent success criteria. The evaluation framework may differ depending on whether the extracted solutes are in the permeate, the retentate, or both. We hope that this analysis provides the theoretical foundation to support future development of NF membranes and processes for various solute-solute separation applications.

# Declarations

# Acknowledgement

The authors acknowledge the support from the US National Science Foundation (#2017998), Water Research Foundation (Paul L. Busch Award to S.L.), US-Israel Binational Agricultural Research and Development Fund, and the National Natural Science Foundation of China (#U20A20139).

# References

1. Zhao, Y. *et al.* Differentiating Solutes with Precise Nanofiltration for Next Generation Environmental Separations: A Review. Environ. Sci. Technol. **55**, 1359–1376 (2021).
2. Epsztein, R., DuChanois, R. M., Ritt, C. L., Noy, A. & Elimelech, M. Towards single-species selectivity of membranes with subnanometre pores. Nat. Nanotechnol. **15**, 426–436 (2020).
3. Werber, J. R., Deshmukh, A. & Elimelech, M. The Critical Need for Increased Selectivity, Not Increased Water Permeability, for Desalination Membranes. Environ. Sci. Technol. Lett. **3**, 112–120 (2016).
4. Elimelech, M. & Phillip, W. A. The future of seawater desalination: Energy, technology, and the environment. Science (80-.). **333**, 712–717 (2011).
5. Park, H. B., Kamcev, J., Robeson, L. M., Elimelech, M. & Freeman, B. D. Maximizing the right stuff: The trade-off between membrane permeability and selectivity. Science (80-.). **356**, 1138–1148 (2017).
6. Werber, J. R., Porter, C. J. & Elimelech, M. A Path to Ultraselectivity: Support Layer Properties to Maximize Performance of Biomimetic Desalination Membranes. Environ. Sci. Technol. **52**, 10737–10747 (2018).
7. Yang, Z., Guo, H. & Tang, C. Y. The upper bound of thin-film composite (TFC) polyamide membranes for desalination. J. Memb. Sci. **590**, 117297 (2019).
8. Yang, Z., Long, L., Wu, C. & Tang, C. Y. High Permeance or High Selectivity? Optimization of System-Scale Nanofiltration Performance Constrained by the Upper Bound. ACS ES&T Eng. **2**, 377–390 (2022).
9. Fang, W., Shi, L. & Wang, R. Interfacially polymerized composite nanofiltration hollow fiber membranes for low-pressure water softening. J. Memb. Sci. **430**, 129–139 (2013).
10. Labban, O., Liu, C., Chong, T. H. & Lienhard V, J. H. Fundamentals of low-pressure nanofiltration: Membrane characterization, modeling, and understanding the multi-ionic interactions in water softening. J. Memb. Sci. **521**, 18–32 (2017).
11. Wang, T., Han, H., Wu, Z., Dai, R. & Wang, Z. Humic Acid Modified Selective Nanofiltration Membrane for Efficient Separation of PFASs and Mineral Salts. ACS ES&T Water **2**, 1152–1160 (2022).
12. Zhao, Y., Tong, X. & Chen, Y. Fit-for-Purpose Design of Nanofiltration Membranes for Simultaneous Nutrient Recovery and Micropollutant Removal. Environ. Sci. Technol. **55**, 3352–3361 (2021).
13. Lin, J. *et al.* Toward Resource Recovery from Textile Wastewater: Dye Extraction, Water and Base/Acid Regeneration Using a Hybrid NF-BMED Process. ACS Sustain. Chem. Eng. (2015). doi:10.1021/acssuschemeng.5b00234

14. Li, X. *et al.* Membrane-based technologies for lithium recovery from water lithium resources: A review. J. Memb. Sci. **591**, 117317 (2019).
15. Woong, J. *et al.* Hydrometallurgy Recovery of lithium from Uyuni salar brine. Hydrometallurgy **117–118**, 64–70 (2012).
16. Swain, B. Recovery and recycling of lithium: A review. Sep. Purif. Technol. **172**, 388–403 (2017).
17. Xu, S. *et al.* Extraction of lithium from Chinese salt-lake brines by membranes: Design and practice. J. Memb. Sci. **635**, (2021).
18. Xu, P., Hong, J., Xu, Z., Xia, H. & Ni, Q. Novel aminated graphene quantum dots (GQDs-NH2)-engineered nanofiltration membrane with high Mg2+/Li + separation efficiency. Sep. Purif. Technol. **258**, 118042 (2021).
19. Yang, Z., Fang, W., Wang, Z., Zhang, R. & Zhu, Y. Dual-skin layer nanofiltration membranes for highly selective Li+/Mg 2 + separation. J. Memb. Sci. **620**, (2021).
20. Bi, Q., Zhang, C., Liu, J., Liu, X. & Xu, S. Positively charged zwitterion-carbon nitride functionalized nanofiltration membranes with excellent separation performance of Mg 2 + / Li + and good antifouling properties. Sep. Purif. Technol. **257**, 117959 (2021).
21. Xu, P. *et al.* "Bridge" graphene oxide modi fi ed positive charged nano fi ltration thin membrane with high e ffi ciency for Mg2+/Li + separation. Desalination **488**, (2020).
22. Shen, Q., Xu, S., Xu, Z.-L., Zhang, H.-Z. & Dong, Z.-Q. Novel thin-film nanocomposite membrane with water-soluble polyhydroxylated fullerene for the separation of Mg2+/Li + aqueous solution. J. Appl. Polym. Sci. 48029 (2019). doi:10.1002/app.48029
23. Guo, C. *et al.* Amino-rich carbon quantum dots ultrathin nanofiltration membranes by double "one-step" methods: Breaking through trade-off among separation, permeation and stability. Chem. Eng. J. **404**, 127144 (2021).
24. He, R. *et al.* Unprecedented Mg2+/Li + separation using layer-by-layer based nanofiltration hollow fiber membranes. Desalination **525**, (2022).
25. Wang, R., Zhang, J., Tang, C. Y. & Lin, S. Understanding Selectivity in Solute – Solute Separation: Definitions, Measurements, and Comparability. Environ. Sci. Technol. (2022). doi:10.1021/acs.est.1c06176
26. Yaroshchuk, A. E. Negative rejection of ions in pressure-driven membrane processes. Adv. Colloid Interface Sci. **139**, 150–173 (2008).
27. Yaroshchuk, A., Bruening, M. L. & Zholkovskiy, E. Modelling nanofiltration of electrolyte solutions. Adv. Colloid Interface Sci. **268**, 39–63 (2019).
28. Yaroshchuk, A., Bruening, M. L., Eduardo, E. & Bernal, L. Solution-Diffusion-Electro-Migration model and its uses for analysis of nanofiltration, pressure-retarded osmosis and forward osmosis in multi-ionic solutions. J. Memb. Sci. **447**, 463–476 (2013).
29. Yaroshchuk, A. & Bruening, M. L. An analytical solution of the solution-diffusion-electromigration equations reproduces trends in ion rejections during nanofiltration of mixed electrolytes. J. Memb.

Sci. **523**, 361–372 (2017).

30. Geise, G. M., Park, H. B., Sagle, A. C., Freeman, B. D. & McGrath, J. E. Water permeability and water/salt selectivity tradeoff in polymers for desalination. J. Memb. Sci. **369**, 130–138 (2011).
31. Ritt, C. L. *et al.* The open membrane database: Synthesis–structure–performance relationships of reverse osmosis membranes. J. Memb. Sci. **641**, (2022).

# Figures

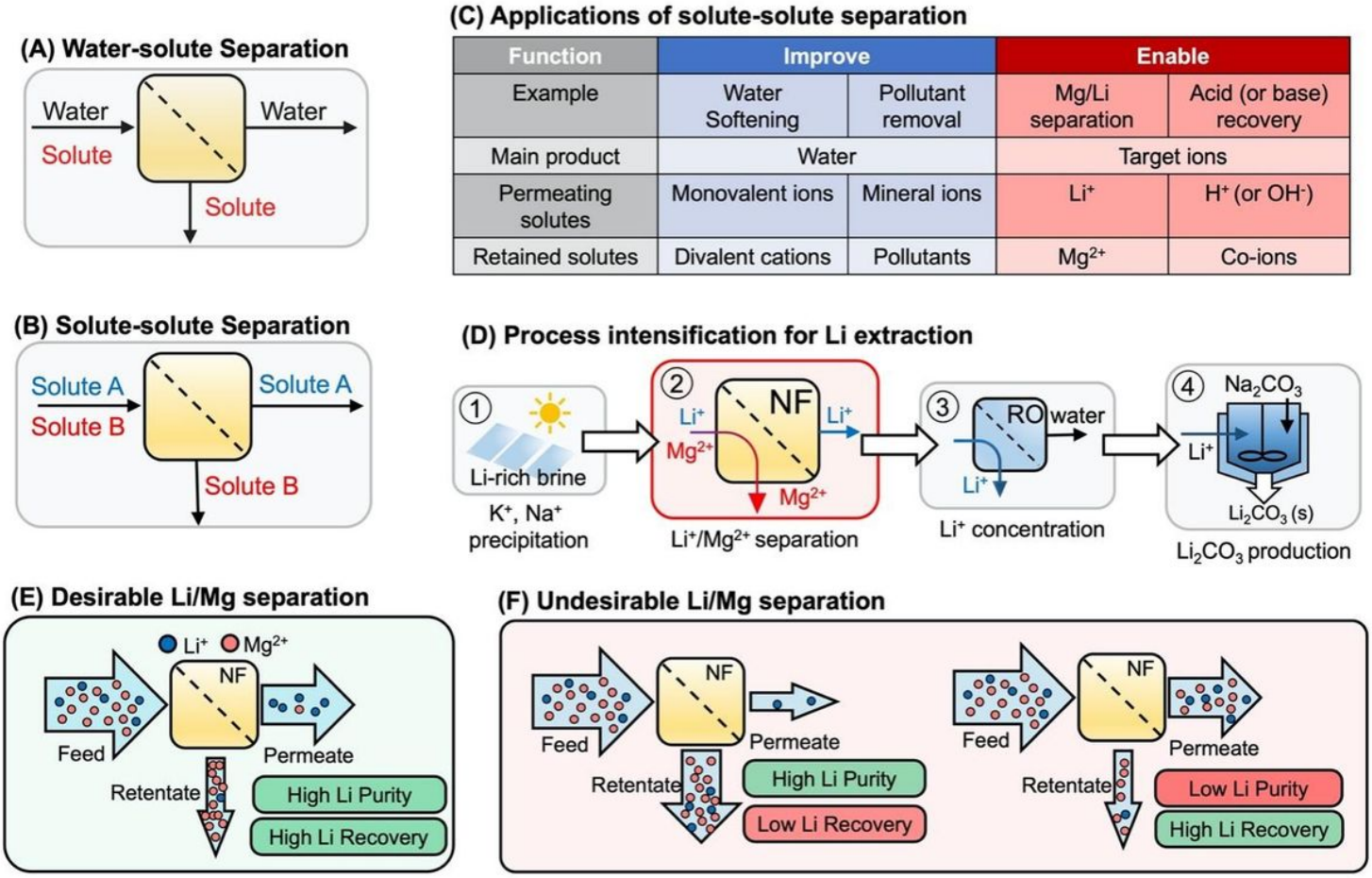


**Figure 1**

**(A)** Illustration of conventional water/solute separation. Water is the primary product whereas the solutes are the unwanted constituents to be rejected by membranes. **(B)** Illustration of solute-solute separation. Certain target solutes are allowed to pass through while the others are retained by membranes. (C) Representative applications of selective solute-solute separation classified into two categories: improvement and enablement. Examples of the improvement category include NF-based water softening and micropollutant removal, where the primary product is water. Examples of the enablement category include acid (or base) recovery and Li/Mg separation, where the primary product is target solute. **(D)** An example treatment-train for Li extraction where NF-based Li/Mg separation is a critical step. An evaporative process first precipitates out Na and K salts and pre-enriches Li concentration; an NF process

next separates Li from Mg, with most Li recovered to the permeate; an RO process then concentrates the Li-rich NF permeate; and a final precipitation process generates $Li_2CO_3$ as the product from the Li-rich RO retentate with $Na_2CO_3$. Success criteria for Li/Mg separation: **(E)** a successful Li/Mg separation should achieve high Li purity and recovery. **(F)** An undesired Li/Mg separation does not attain high Li purity and recovery simultaneously.

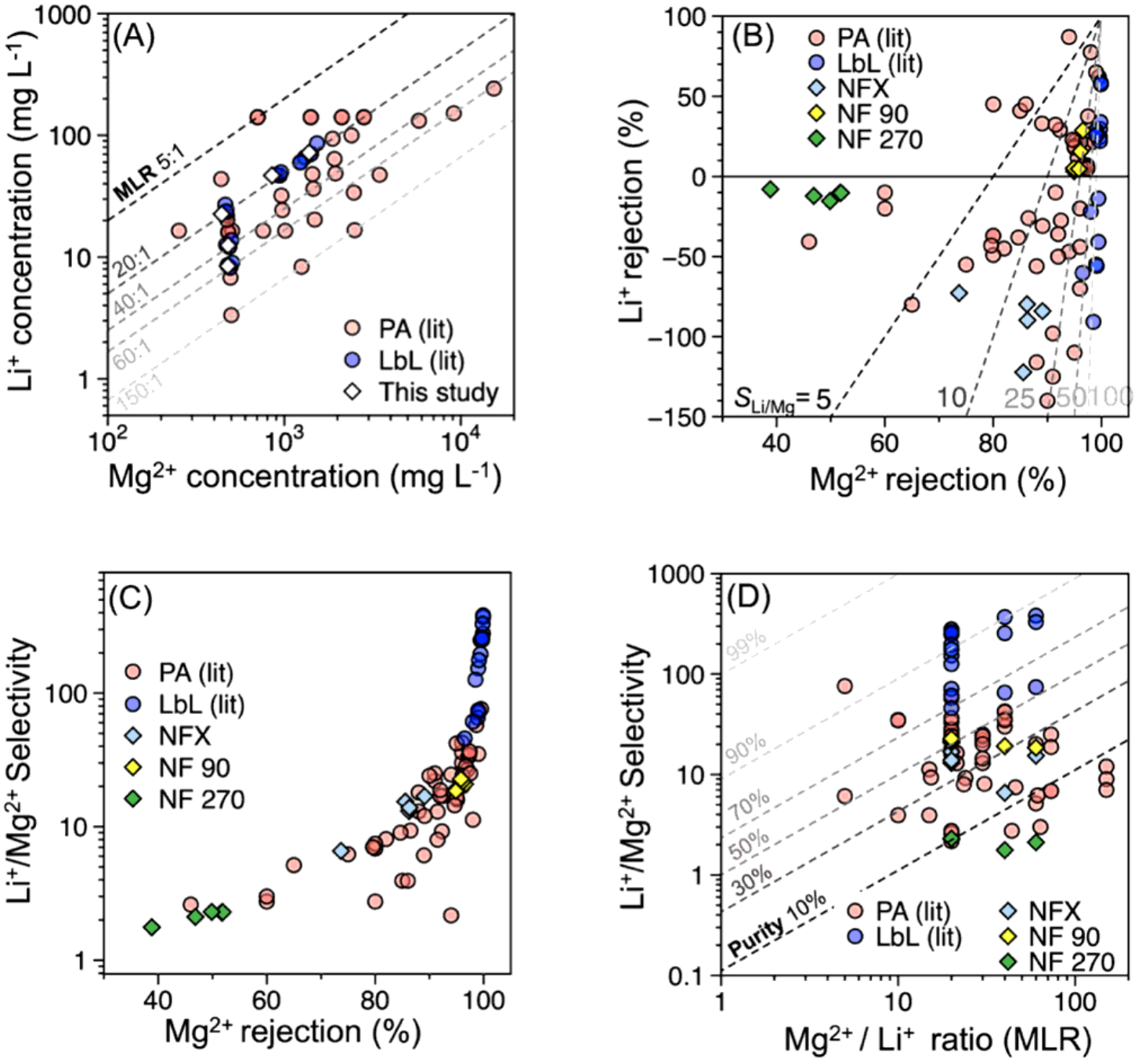


**Figure 2**

**(A)** $Li^+$ and $Mg^{2+}$ concentrations of the feed waters used in this study and studies reported in the literature, with the $Mg^{2+}/Li^+$ mass ratios (MLR) presented in dash lines (vary from 5:1 to 150:1). Data points on the same dash line have the same MLR. **(B)** $Li^+$ and $Mg^{2+}$ rejections of three commercial NF

membranes tested in this study (NFX, NF90, and NF270) and membranes reported in the literature, with $Li^+/Mg^{2+}$ selectivity (defined by Eq. 1) values presented in dash lines (vary from 5 to 100). Data points on the same dash line have the same $Li^+/Mg^{2+}$ selectivity. **(C)** $Li^+/Mg^{2+}$ selectivity as a function of $Mg^{2+}$ rejection for three commercial NF membranes tested in this study and membranes reported in the literature. The selectivity has a strong dependence on $Mg^{2+}$ rejection, especially when $Mg^{2+}$ rejection is high. **(D)** $Li^+/Mg^{2+}$ selectivity as a function of MLR, with the permeate Li purity (defined by Eq. 2) presented in dash lines (varies from 10% to 99%). Data points on the same dash line have the same purity. For all panels, circles represent data from literature studies, including polyamide membranes (legend: PA) and polyelectrolyte membranes fabricated by layer-by-layer deposition (legend: LbL); diamonds represent data collected in this study.

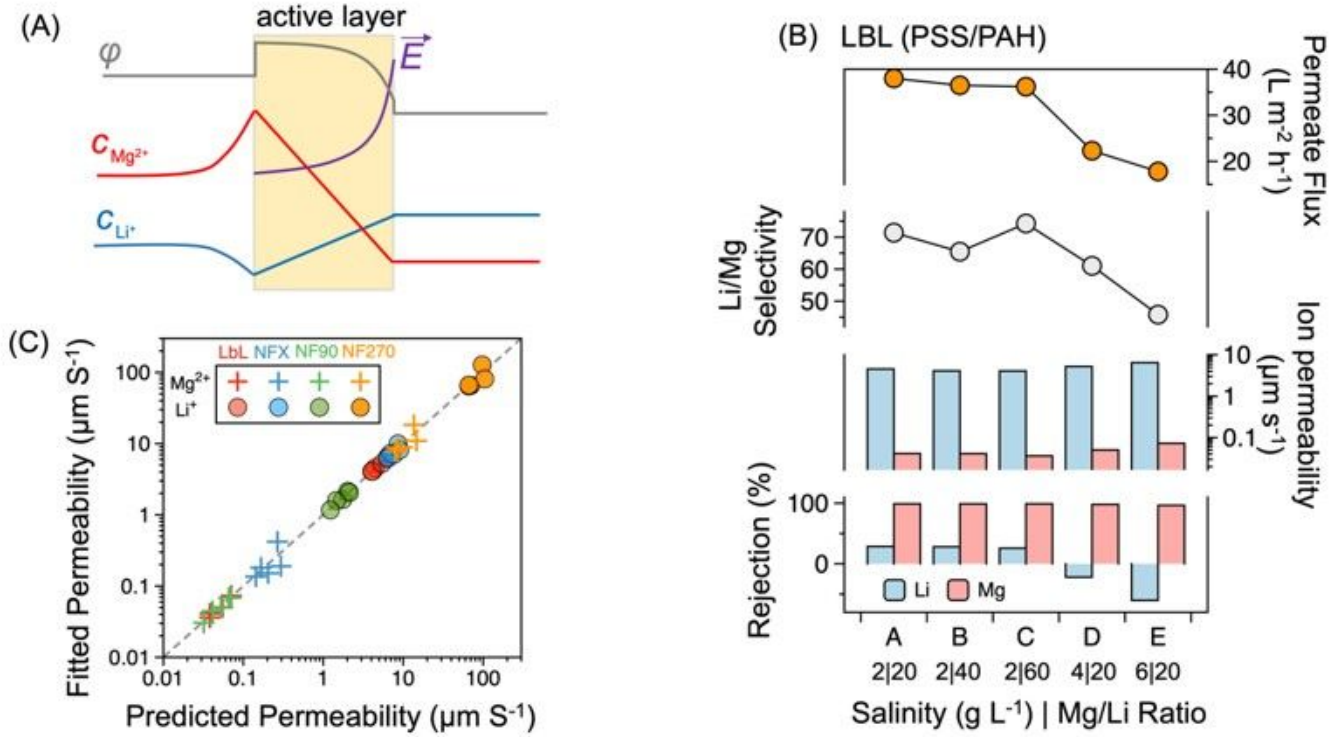


**Figure 3**. **(A)** Representative distributions of electrical potential (φ), electric field ($\vec{E}$), and concentrations of $Mg^{2+}$ ($c_{Mg^{2+}}$) and $Li^+$ ($c_{Li^+}$) across the active layer of a positively charged NF membrane. **(B)** From top to bottom: permeate water flux, $Li^+/Mg^{2+}$ selectivity, fitted ion permeabilities, and measured rejections as a function of feed composition. The composition comprises both total concentration (g $L^{-1}$) and $Mg^{2+}/Li^+$ (mass) ratio. Rejections and flux data were reported in He et al.'s study.[24] $Li^+/Mg^{2+}$ selectivity was calculated with Eq. 1. Ion permeabilities were fitted with the solution-diffusion-electromigration (SDEM) model. **(C)** Fitted permeability extracted from the SDEM model using experimental data vs. the predicted permeability obtained using the empirical correlation presented in Eq. 6 for three commercial NF membranes tested in this study and the LbL polyelectrolyte membrane in He et al.'s study[24]. Concentration polarization was accounted for by an assumed mass transfer coefficient of 100 L $m^{-2}$ $h^{-1}$ for both LiCl and $MgCl_2$.

## Figure 3

See image above for figure legend.

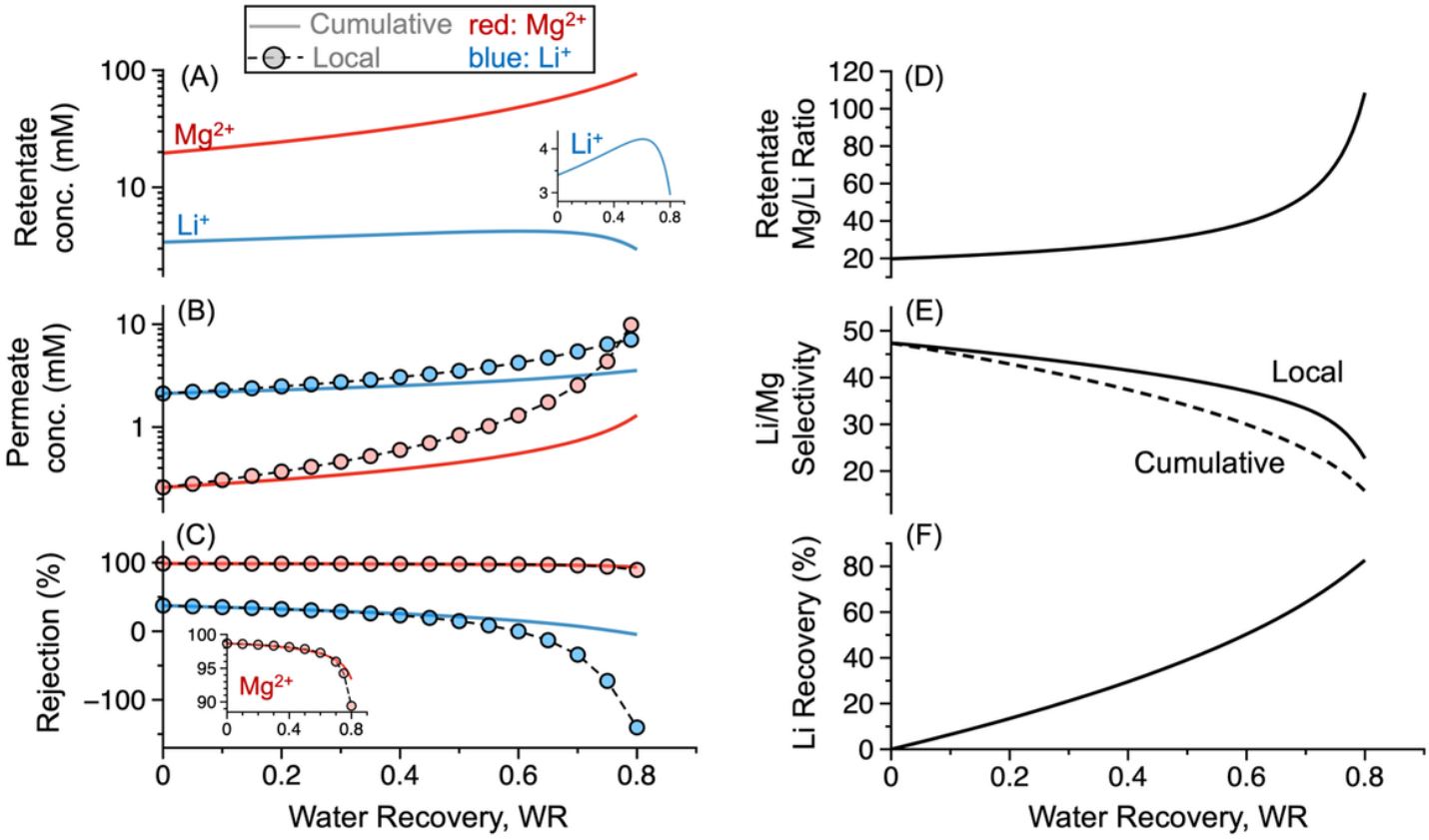


## Figure 4

**(A)** Retentate concentrations (inset is the magnified $Li^+$ curve), **(B)** Permeate concentrations, and **(C)** Rejections (inset is the magnified $Mg^{2+}$ curve) as a function of water recovery (WR). The dash curves with circles represent “local values” whereas the solid curves present “cumulative values”. In panel B, for example, the local concentration is obtained by applying the SDEM model to a differential module element using the retentate concentration at the same position (as in panel A); whereas the cumulative average concentration is obtained considering accumulation of ions from the permeate stream entering the differential module element. In panel C, the local and cumulative rejections are calculated using the local and cumulative concentrations in panel B, respectively. On the right: **(D)** Retentate Mg/Li ratio (MLR), **(E)** Local and cumulative Li/Mg selectivity, and **(F)** Li recovery as a function of WR. Simulation used 6 bar and a feed solution of LiCl and $MgCl_2$ with 2 g $L^{-1}$ total concentration and MLR of 20. Concentration polarization was accounted for by a mass transfer coefficient of 100 L $m^{-2}$ $h^{-1}$ for both LiCl and $MgCl_2$.

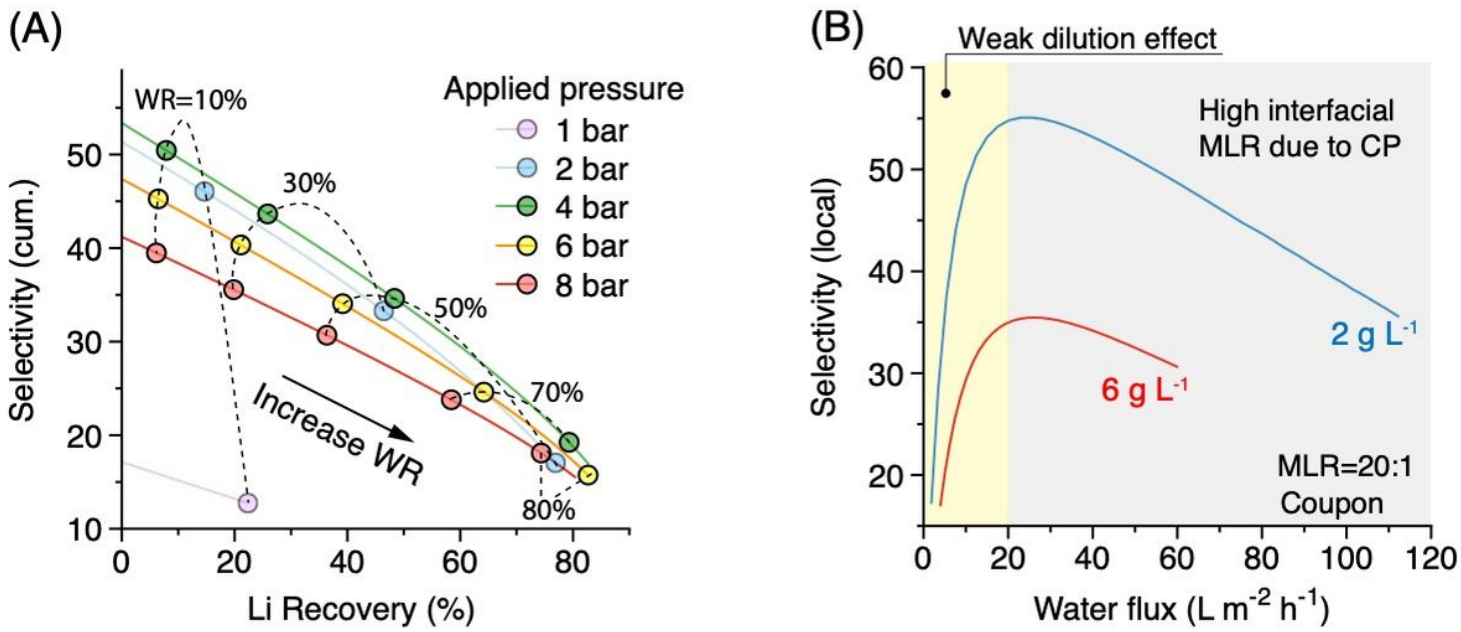


**Figure 5**

**(A)** Tradeoff between cumulative selectivity and Li recovery at different applied pressures. At a given pressure, the Li recovery increases when more water is recovered. The values of water recovery (WR) are also provided. Each dash curve connects data points from the same WR obtained using different applied pressures. The simulations were performed using an applied pressure of 1, 2, 4, 6 and 8 bar and a feed solution of LiCl and $MgCl_2$ with 2 g $L^{-1}$ total concentration and an MLR of 20. **(B)** Coupon-scale selectivity as a function of water flux with a feed MLR of 20 and a total concentration of 2 g $L^{-1}$ and 6 g $L^{-1}$. The applied pressure varies up to 10 bar to vary the water flux. Concentration polarization was accounted for by an assumed mass transfer coefficient of 100 L $m^{-2}$ $h^{-1}$ for both LiCl and $MgCl_2$.

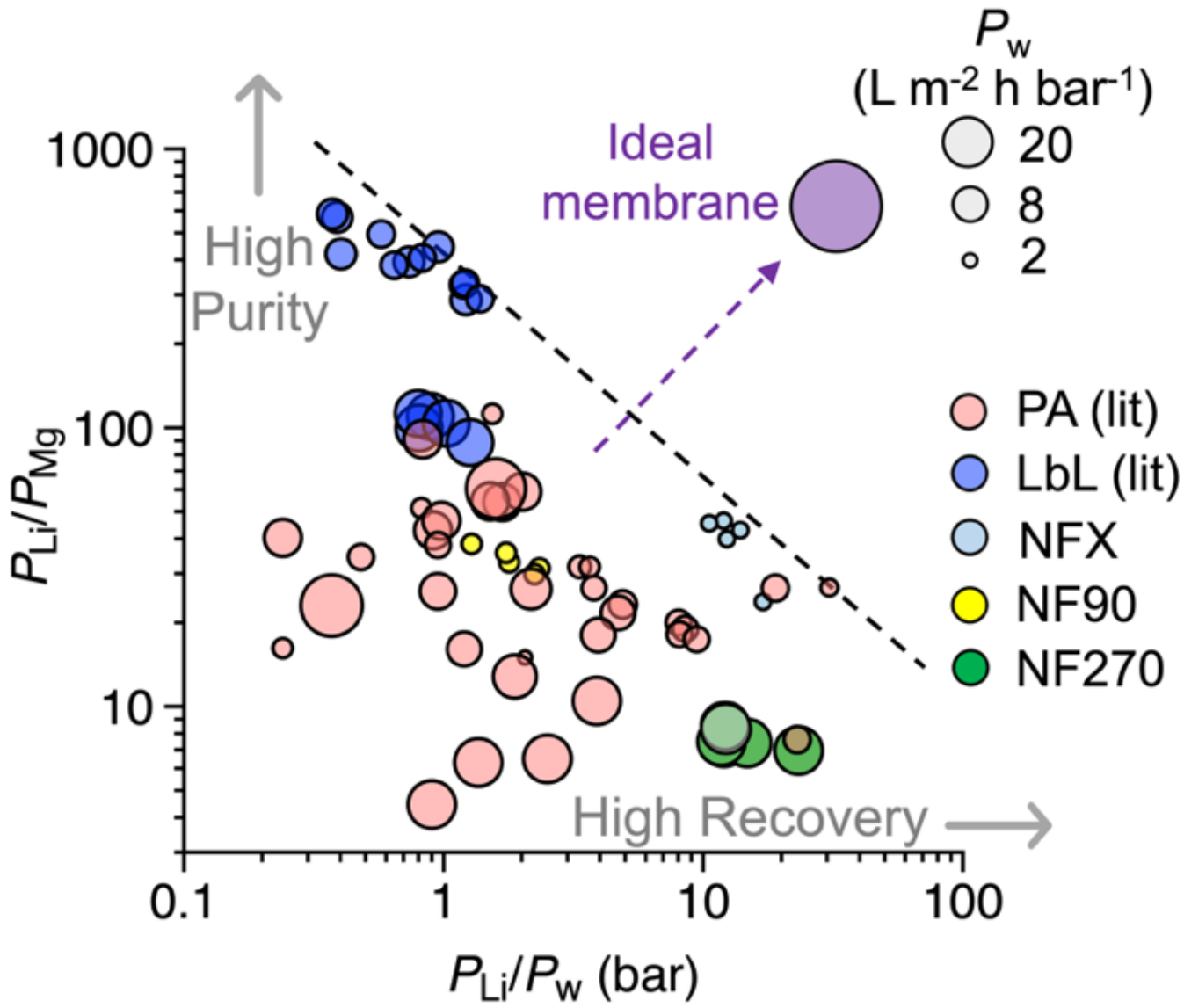


**Figure 6**

Ratio between Li permeability and Mg permeability ($P_{Li}/P_{Mg}$) vs. ratio between Li permeability and water permeability ($P_{Li}/P_w$). The size of the data points quantifies the water permeability, $P_w$ (see legend). Increasing $P_{Li}/P_w$ improves Li recovery, whereas increasing $P_{Li}/P_{Mg}$ enhances permeate Li purity. The permeabilities are extracted using the SDEM model with an assumed mass transfer coefficient of 100 L m$^{-2}$ h$^{-1}$ for both LiCl and $MgCl_2$.

## Supplementary Files

This is a list of supplementary files associated with this preprint. Click to download.

- SupportingInformationWangetalsoluteseparationNatureWatersubmission.docx